ISSN 1062-8738, Bulletin of the Russian Academy of Sciences: Physics, 2024, Vol. 88, No. 7, pp. 1140–1147. © Pleiades Publishing, Ltd., 2024.

Synthesis and Magnetic Properties of $Fe_{1.1}Ga_{0.9}O_3$, Measured According to Electron Spin Resonance

I. V. Yatsyk[a, *], R. M. Eremina[a], E. M. Moshkina[b], R. G. Batulin[c], and A. V. Shestakov[d]

[a] *Zavoiskii Physical-Technical Institute, Federal Research Center "Kazan Scientific Center," Russian Academy of Sciences, Kazan, 420029 Russia*

[b] *Kirensky Institute of Physics, Federal Research Center "Krasnoyarsk Scientific Center," Siberian Branch, Russian Academy of Sciences, Krasnoyarsk, 660036 Russia*

[c] *Institute of Physics, Kazan Federal University, Kazan, 420008 Russia*

[d] *Prokhorov General Physics Institute, Russian Academy of Sciences, Moscow, 119991 Russia*

**e-mail: i.yatzyk@gmail.com*

Received February 19, 2024; revised March 18, 2024; accepted March 29, 2024

Abstract—The authors study the formation of crystals of Fe-Ga oxides and Fe–Ga–Cu borates in a multicomponent flux system based on $Bi_2Mo_3O_{12}$–$Na_2B_4O_7$. The Curie–Weiss temperature ($\theta_{CW} = 289$ K) and the temperature of the ferrimagnet–paramagnet phase transition ($T_C = 288$ K) are determined from the electron spin resonance (ESR) spectrum and the magnetization of an $Fe_{1.1}Ga_{0.9}O_3$ single crystal, depending on temperature. Lines of spin-wave resonance are observed in the spectrum of magnetic resonance in the ordered phase.

Keywords: flux crystal growth, phase diagram, electron spin resonance, ferrimagnets, spin-wave resonance

DOI: 10.1134/S1062873824707220

INTRODUCTION

Transition metal oxides and borates, including ones containing Cu, Fe and Ga cations, are basic materials and have a strong potential for application, diverse properties, and a wide variety of crystal structures. An important feature of such compounds in relation to the above cations (particularly trivalent Fe^{3+} and Ga^{3+}) is in many cases a continuous series of solid solutions. Replacing the paramagnetic Fe^{3+} cation with the diamagnetic Ga^{3+} cation allows us to control the properties of compounds, largely by changing a ratio between the cations [1–14].

Among iron and gallium oxides, we can identify a region of the phase diagram that includes the transition from the hematite α-Fe_2O_3 phase to the monoclinic β-Ga_2O_3 phase through a series of $Fe^{3+} \rightarrow Ga^{3+}$ substitutions. However, such transitions occur through the orthorhombic $Fe_{2-x}Ga_xO_3$ phase, rather than directly. The orthorhombic $Fe_{2-x}Ga_xO_3$ crystals are promising magnetoelectric multiferroics [8–12, 14]. The magnetic and magnetoelectric properties of these compounds depend strongly on concentration x. The region of stability in this phase ranges from $x = 0.6$ to $x = 1.2$, depending on concentration [9]. This compound is also interesting from a structural viewpoint because there are four nonequivalent positions occupied by iron and gallium cations. According to different literature sources, the occupancy of these positions by Fe/Ga cations also changes, depending on how a sample is prepared, since this affects the temperature of ferrimagnetic ordering [9].

Adding a divalent Cu^{2+} subsystem to an Fe–Ga system greatly expands the range of the structures and properties of the considered compounds, which also form a continuous series of Fe-Ga solid solutions [15, 16]. From the viewpoint of growth in this work, such solid solutions are monoclinic ludwigites $Cu_2Fe_{1-x}Ga_xBO_5$.

Orthorhombic $Fe_{2-x}Ga_xO_3$ and ludwigites $Cu_2Fe_{1-x}Ga_xBO_5$ both contain four nonequivalent cationic positions in their structures, which allows the potentialities of complicated variants to arise in magnetic ordering. Working with solid solutions requires complete control over the composition of cations at the growth stage by managing the conditions for obtaining samples. In this work, we used a flux technique approach to ensure such conditions. This allowed us to observe the simultaneous crystallization of several phases (if, e.g., we were crossing a phase boundary) with no loss in the quality and size of the samples, and to prepare samples of different compositions based on the same flux with successive additions [17, 18]. The correct choice of solvent allows the building of intermediate chemical bonds in the

flux system (between the solvent and the dissolved components) to control the composition of the crystal [18].

This work presents results from studying the magnetic properties of orthorhombic $Fe_{1.1}Ga_{0.9}O_3$, obtained using electron spin resonance (ESR) and magnetometry to investigate the formation of phases upon the crystallization of Fe–Ga oxides and borates in a multicomponent melt–solution system based on $Bi_2Mo_3O_{12}$–$Na_2B_4O_7$.

EXPERIMENTAL

We used a flux technique approach to perform our growth experiments. Fluxes were prepared in a platinum crucible ($V = 100$ cm^3) at a temperature of $T =$ 1100°C through sequential melting of the components of the flux system. The prepared melt solutions were kept at a temperature of $T = 1100$°C for 3 h. We then assessed the formation of crystals and studied the sequence of high-temperature crystallizing phases (HTCP). To grow single-crystalline samples after the search stage, the temperature in the furnace was first rapidly reduced at a rate of 200°C/h to attain an initial temperature of $T_{start} = (T_{sat} - 5)$°C. It was then lowered slowly at a rate of 1 to 4°C a day. After the end of the growth stage, the resulting single crystals were separated from the remaining melt solution via etching in a 20% aqueous solution of nitric acid HNO_3.

Measurements of the ESR spectra of $Fe_{2-x}Ga_xO_3$ crystals in the form of needles with dimensions of $3 \times 0.2 \times 0.2$ mm^3 were confirmed on a VarianE-12 X ESR spectrometer (in the MW range of 9.4 GHz) equipped with an ER 4131VT resonator, nitrogen purging, and the possibility of changing the temperature from 300 to 700 K. The angular dependences of the ESR spectra were measured on a Bruker ER 200 SRC ESR spectrometer (EMX/plus) at a frequency of 9.4 GHz. The ESR spectra were registered in the 294 to 448 K range of temperatures.

Magnetization was measured with a PPMS-9 magnetometer in the 10 to 300 K range of temperatures in the field cooling (FC) and zero-field cooling (ZFC) modes. The magnetic hysteresis loops were measured in a range of fields up to 5 T.

X-ray fluorescence analysis (XRFA) with a Bruker S2 Ranger X-ray fluorescence spectrometer was used to clarify the stoichiometric formula of a single crystal.

STUDYING FEATURES OF MELT–SOLUTION CRYSTALLIZATION FOR Fe–Ga OXIDES AND Fe–Ga–Cu BORATES

As noted above, the choice of the solvent plays a key role when working with the flux technique approach. Due to the importance of controlling the composition of Fe–Ga and Fe–Ga–Cu solid solutions, we must study the effect the components of the solvent might have on the composition of the crystallized substance. The considered initial flux system had the form

$$(100 - n)\ \text{wt}\ \%(Bi_2Mo_3O_{12} + Na_2B_4O_7) + n\ \text{wt}\ \%(2CuO + 0.5Fe_2O_3 + 0.5B_2O_3). \quad (1)$$

System (1) was designed for the stoichiometry of ludwigite Cu_2FeBO_5 as a crystal-forming material and contained no gallium oxide Ga_2O_3 at the initial stage. The solvent was a mixture of $Bi_2Mo_3O_{12}$–$Na_2B_4O_7$, with no additions of boron oxide B_2O_3 in excess of the borax stoichiometry ($Na_2B_4O_7$). At the initial stage, the concentration of crystal-forming component n was 33%.

Using similar systems for Mn-containing ludwigites, it was shown in [18] that oxide MoO_3 has a strong effect on a phase containing Mn^{2+} cations, while oxide Na_2O (or borax $Na_2B_4O_7$) affects a phase containing Mn^{3+} cations. The fraction of borax $Na_2B_4O_7$ per weight % of Fe_2O_3 in system (1) was calculated in a manner similar to how the ratio of $Na_2O/Mn_2O_3 = 1$ was calculated in [18] (in accordance with the possible formation of such intermediate chemical species as $NaFeO_2$ and $NaMnO_2$). However, the formation of crystals in system (1) differs considerably from in the manganese-containing system studied earlier, due possibly to different temperatures of the decomposition of such trioxides as Mn_2O_3 and Fe_2O_3. This happens because the temperature of decomposition characteristic of Mn_2O_3 with the loss of oxygen and the formation of oxide Mn_3O_4 with manganese simultaneously in valence states 2+ and 3+ lie in the 900 to 1100°C range of operating temperatures, while Fe_2O_3 oxide remains stable at much higher temperatures.

The valence of the Fe^{3+} cation thus remains stable, in contrast to the changing valence of the manganese cations. This greatly affects the sequence of the high-temperature crystallizing phase (HTCP). Despite the possibility of Fe^{2+} cations entering the structure of molybdate, which is isostructural with respect to $Mn^{2+}MoO_4$, phase $Fe^{2+}MoO_4$ does not form in system (1), as was shown in [18] from the existence of $Mn_{1-x}Fe_xMoO_4$ solid solutions. The HTCP of initial system (1) is represented by hematite phase α-Fe_2O_3 containing only Fe^{3+} cations, despite the stoichiometry of ludwigite in the crystal-forming part. Since the solubility of copper and boron oxides greatly exceeds that of Fe_2O_3, the probability of Fe_2O_3 entering the crystalline phase grows, in contrast to that of CuO and B_2O_3. Only the iron-containing hematite phase crystallizes.

At the next stage, oxide CuO was introduced into flux system (1) in the ratio $Bi_2Mo_3O_{12}$: CuO = 1 : 0.5. This modification of the flux's composition allowed us to change the HTCP toward a copper-containing spinel phase (e.g., Cu_2FeBO_5). The next shift of HTCP

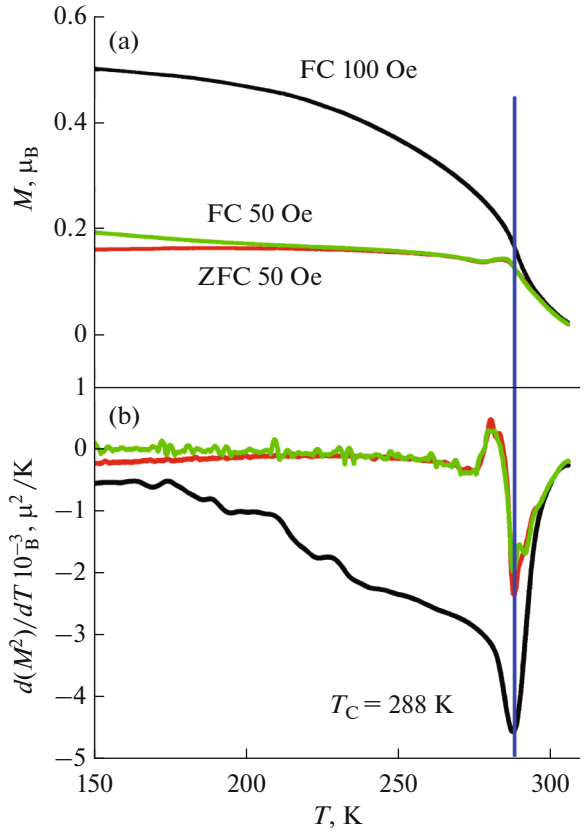

Fig. 1. Temperature dependences for $Fe_{1.1}Ga_{0.9}O_3$: (a) magnetization (FC and ZFC mode); (b) $\partial(M^2)/\partial T$ in the orientation when the magnetic field is parallel to the c axis of the crystal.

toward a ludwigite phase occurred after raising the proportion of copper oxide to $Bi_2Mo_3O_{12}$: CuO = 1 : 1. An iron–copper ludwigite phase from a flux based on $Bi_2Mo_3O_{12}$–$Na_2B_4O_7$ can therefore crystallize when oxide CuO is introduced into the solvent above the stoichiometry of ludwigite.

It was shown in [16] that copper-gallium ludwigite Cu_2GaBO_5 can be prepared from such melt solutions without the need to add copper oxide in excess of stoichiometry. At the next stage, oxides Ga_2O_3 and B_2O_3 were added to a melt solution in order to remove all excess copper from the solvent. The new flux system can therefore be described as

$$(100 - n)\ \text{wt}\ \%(Bi_2Mo_3O_{12} + Na_2B_4O_7) + n\ \text{wt}\ \%(0.72Cu_2FeBO_5 + 0.28Cu_2GaBO_5). \quad (2)$$

Concentration n in this system was n = 31%. The crystallization of two phases was observed: ludwigite $Cu_2Fe_{1-x}Ga_xBO_5$ and orthorhombic $Fe_{2-x}Ga_xO_3$. No copper was introduced into the solvent, as in the case of system (1) with no gallium oxide in the melt solution. The concentration of oxide Ga_2O_3 was then raised to the limit ratio Fe : Ga = 3 : 2, which corresponds to the limit of stability of the orthorhombic $Fe_{2-x}Ga_xO_3$ phase. This system's HTCP was represented by the $Fe_{2-x}Ga_xO_3$ phase. Single crystals of this compound were obtained via crystallization. The temperature of melt solution saturation was T_{sat} = 980°C, the rate at which the temperature was reduced was dT/dt = 8°C/day, and the period of growth was 24 h. The resulting crystals were black orthogonal prisms with a maximum size of 3 × 0.2 × 0.2 mm^3.

The phase composition of the obtained crystals was monitored via X-ray diffraction analysis. The true chemical composition of orthorhombic $Fe_{2-x}Ga_xO_3$ (ratio Fe/Ga) was studied by means of X-ray phase analysis, which showed a uniform distribution of iron and gallium in each sample. Nine points in a single crystal chosen to study its magnetic properties were analyzed to obtain the most objective results. The true composition of this compound corresponded to formula $Fe_{1.1}Ga_{0.9}O_3$. The true Fe/Ga ratio was therefore lower than the similar ratio characteristic of the introduced mixture, which is consistent with the difference between the coefficients of the distribution of Fe_2O_3 and Ga_2O_3 oxides in the studied melt solutions. Gallium oxide was therefore characterized by lower solubility, due to which gallium enters the crystallizing phase in much greater amounts than iron does. A similar mechanism could be used to analyze the transition to the orthorhombic $Fe_{2-x}Ga_xO_3$ phase from the ludwigite phase by comparing the solubilities of B_2O_3, CuO, and Ga_2O_3.

MAGNETIC PROPERTIES OF $Fe_{1.1}Ga_{0.9}O_3$

A single-crystal sample of $Fe_{1.1}Ga_{0.9}O_3$ has the shape of a needle where axis c is directed along the needle itself, and plane ab is perpendicular to the needle.

The temperature dependences of magnetization were obtained in the 4.2 to 304 K range of temperatures and a magnetic field of H = 50, 100 Oe (Fig. 1a). These curves correspond qualitatively to results obtained in [19] for $FeGaO_3$. An abrupt increase in magnetization that corresponds to a ferrimagnetic phase transition is already observed at room temperature. Depending on the magnitude of the applied field, the bifurcation of the FC and ZFC curves is observed in a wide range of temperatures below that of the transition. The smooth bending and subsequent growth of the FC curve are observedelow the point of bifurcation (the temperature corresponding to the divergence of the FC and ZFC curves).

In order to more accurately determine the temperature of the ferrimagnetic phase transition, dependences $\partial M^2/\partial T(T)$ were constructed in proportion to the magnetic contribution to the heat capacity for ferromagnets [20]. The resulting curves are presented in Fig. 1b.

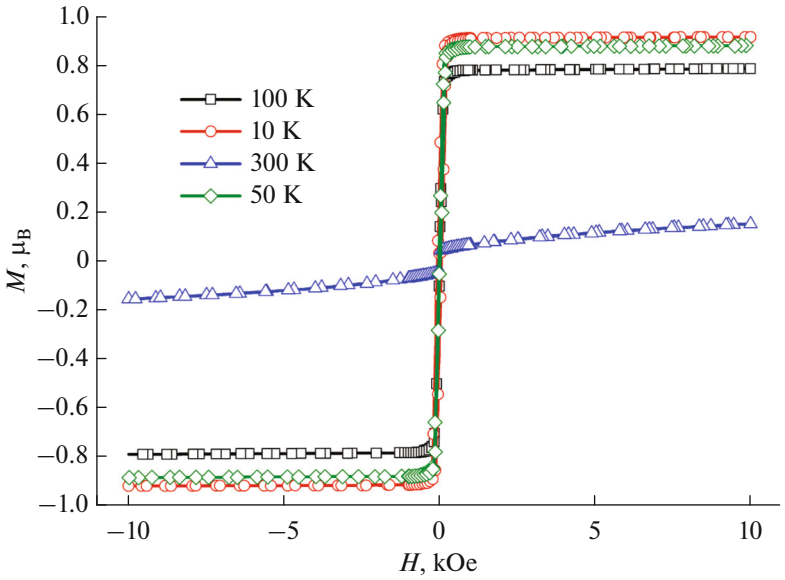

Fig. 2. Magnetic field dependences of magnetization for $Fe_{1.1}Ga_{0.9}O_3$.

We used dependences $\partial M^2/\partial T(T)$ to clarify temperature T_C of the ferrimagnetic phase transition. This approach normally taken to analyze the magnetic properties of ferromagnets, since it has proven itself in analyzing ferrimagnetic systems [20–22]. Compared to the way of determining the temperature of phase transitions for antiferromagnets, where we must analyze the $\partial(\chi T)/\partial T(T)$ dependence [22–24], the resulting curves allow us to obtain unambiguous values at a sufficient level of accuracy.

According to the temperature dependences of the derivative of squared magnetization, the temperature of the ferrimagnetic phase transition was $T_C = 288$ K, based on results from magnetometry.

Field dependences of the magnetization of $Fe_{1.1}Ga_{0.9}O_3$ are presented in Fig. 2. Below temperature T_C, the field dependences are nearly rectangular loops with vertical walls and are characterized by a low coercive force of 60 Oe at a temperature of $T = 10$ K. Beyond the field hysteresis, magnetization reaches the level of saturation and remains constant in the measured range of fields.

The magnetic moment of sample saturation determined from the field dependences of magnetization was no more than 0.9 μ_B, considerably less than the calculated value of $\mu_{eff} = 6.2\ \mu_B$. This deviation can be explained by a ferrimagnetic state of the substance arising. This problem requires that more detailed studies on magnetic behavior be planned in the future.

The angular dependence of the electron spin resonance spectra was measured in two orientations, with (1) the external magnetic field lying in plane *ab* (Fig. 3a) and (2) the external magnetic field lying in plane *bc* (Fig. 3b).

Two intense lines with an abrupt angular dependence were observed in the ESR spectrum for plane *ab*. The intensity of the ESR spectrum lines reached a minimum around 80°, and the position of the resonant field shifted to strong fields. The second ESR line was not registered in the above range of fields (from 0 to 1.4 T). This direction presumably corresponds to axis *b*, so 170° corresponds to the direction of axis *a*.

Figure 3b shows the evolution of the spin resonance line as a function of the angle in plane *bc*. Only one ESR line was registered. The shape of the line was approximated according to the relation

$$\frac{\partial P}{\partial H} = \frac{\partial}{\partial H}\left[\frac{\Delta H + \alpha(H - H_{res})}{(H - H_{res})^2 + \Delta H^2} + \frac{\Delta H + \alpha(H + H_{res})}{(H + H_{res})^2 + \Delta H^2}\right], \quad (3)$$

where H_{res} is the position of the resonance line, ΔH is the linewidth, and α is the parameter of line asymmetry [25].

We obtained angular dependences for the resonant field and ESR linewidth by analyzing the shape of the line (Fig. 4). At 70°, there was an abrupt increase in the ESR linewidth and the resonant field (up to 700 mT). We may assume this angle corresponds to axis *b*.

The angular dependence of the resonant magnetic field is described by the relation for ferromagnetic regions [26]:

$$\left(\frac{\omega}{\gamma}\right)^2 = \left[H_{0z} + 2H_{A1}\sin^2 2\theta_0 + H_{A2}\sin^2 2\theta_0\right] \times \left[H_{0z} + 2H_{A1}\cos 2\theta_0 + 4H_{A2}\sin^2\theta_0\left(1 + 2\cos 2\theta_0\right)\right], \quad (4)$$

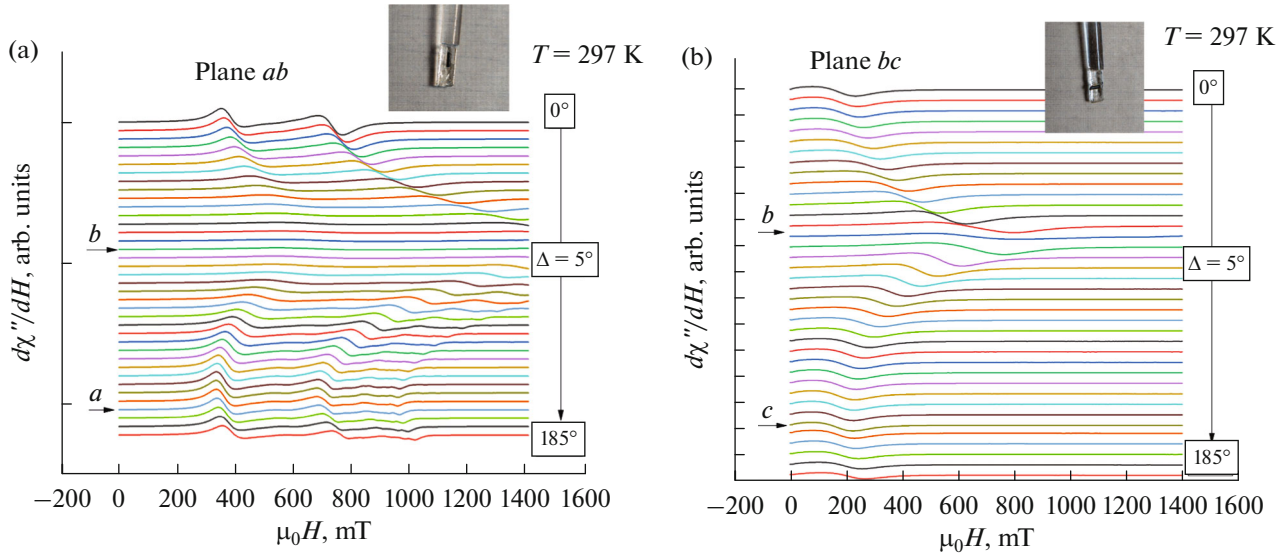

Fig. 3. Evolution of the ESR line as the angle for $Fe_{1.1}Ga_{0.9}O_3$ changes at room temperature (297 K) in (a) plane *ab* and (b) plane *bc*.

where $H_{A1} = K_1/M_0$ and $H_{A2} = K_2/M_0$ are magnetic fields of anisotropy, and H_{0z} is the projection of the magnetic field H_z onto the direction of M_0. Approximating the angular dependence of the resonant value of the magnetic field, we obtained parameters $H_{0z} = 15.2 \pm 0.2$ mT, $H_{A1} = 4.9 \pm 0.2$ mT, and $H_{A2} = -1.8 \pm 0.2$ mT.

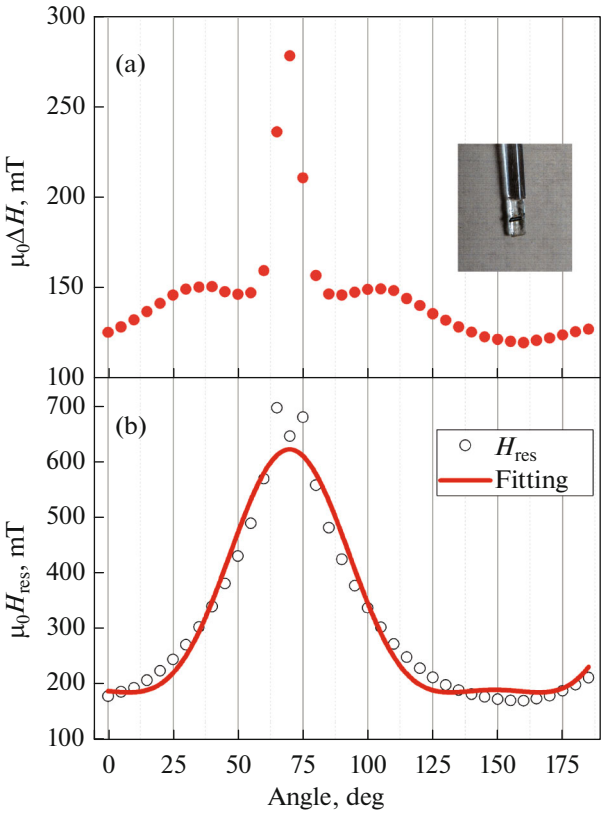

Fig. 4. Angular dependence of (a) ESR linewidth and (b) the magnetic field of resonance for $Fe_{1.1}Ga_{0.9}O_3$ at room temperature (297 K) in plane *bc*.

The ESR spectra were measured when the temperature was changed from 250 to 448 K. The position of the crystal with respect to the external field was chosen so that the line of the ESR spectrum was in the lowest fields. This direction presumably corresponds to that of axis *a*. The evolution of the line of the ESR spectrum as the temperature changed is presented in Fig. 5. The spectrum was registered at a temperature of 250 K in a strong field (1.4 T). The line shifted to a low field (330 mT) as the temperature rose, while its intensity grew to a maximum at a temperature of 320 K. The intensity then fell in inverse proportion to the temperature. Two spectral lines occurring at a room temperature and exhibiting an angular dependence were clearly seen at a temperature of 280 K. As the temperature rose, the lines tended to a resonant field of around 330 mT and coincided with one another. The ESR spectral line then behaved as a single line.

Relation (3) was used to approximate the shape of the line upon a change in temperature. The temperature dependences of the experimental spectra and their approximations are presented in Fig. 6. It should be noted that the characteristic intensity is inversely proportional to the temperature, obviously following the Curie–Weiss law. By comparing the characteristic intensity to the susceptibility of a sample at the same temperature, we can normalize the former and plot the temperature dependence of inverse magnetic susceptibility (Fig. 7). The values of Curie constant $C = 2.28$ K/(cm^3 mol) and Curie–Weiss temperature

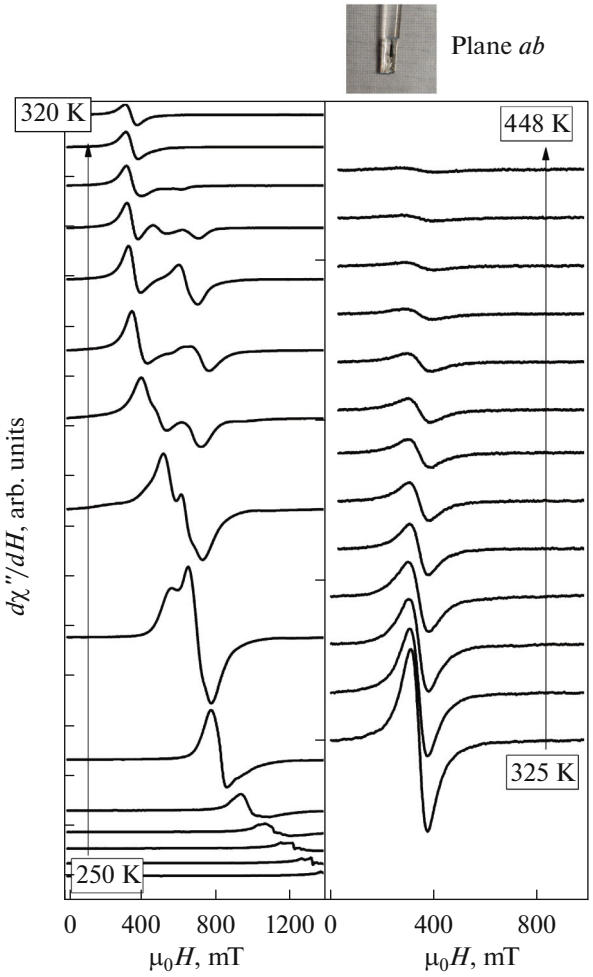

Fig. 5. Evolution of a line in the ESR spectrum as the temperature for $Fe_{1.1}Ga_{0.9}O_3$ changes at an angle of 160° in plane *ab*.

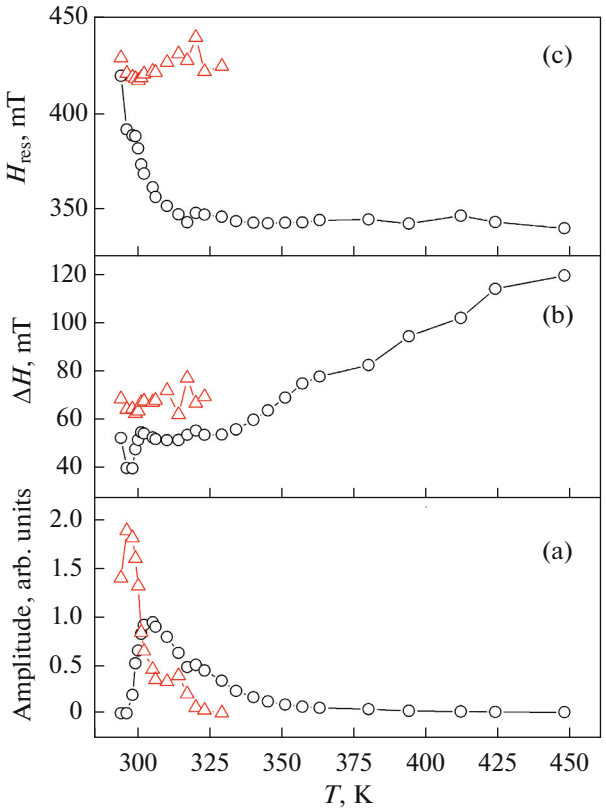

Fig. 6. Temperature dependence of (a) integral intensity, (b) ESR linewidth, and (c) the magnetic field of resonance for $Fe_{1.1}Ga_{0.9}O_3$ in plane *ac*.

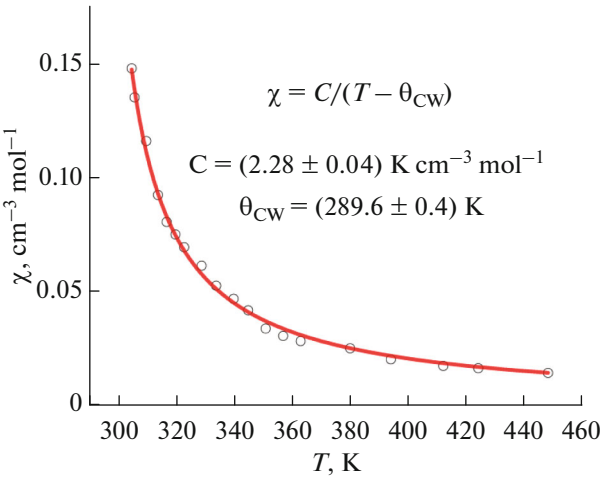

Fig. 7. Temperature dependence of the magnetic susceptibility of $Fe_{1.1}Ga_{0.9}O_3$ in the 300 to 450 K range of temperatures.

$\theta_{CW} = 289$ K were determined by approximating the resulting dependence with a straight line.

Many additional lines that could not be explained through a single paramagnetic or ferromagnetic center were observed upon a detailed examination of the angular dependence of the obtained ESR spectra (Fig. 8). However, we may assume that such signals were due to the effect of spin-wave resonance [26, 27]. A more detailed and in-depth analysis of this phenomenon requires a separate study.

CONCLUSIONS

By studying the formation of crystals in a $Bi_2Mo_3O_{12}$–$Na_2B_4O_7$–B_2O_3 flux system after adding a mixture of Fe_2O_3–CuO–Ga_2O_3 oxides with different contents of gallium oxide, we obtained a series of high-temperature crystallizing phases and single-crystalline samples that included hematite α-Fe_2O_3, spinel $CuFe_2O_4$, ludwigite $Cu_2Fe_{2-x}Ga_xBO_5$ and orthorhombic $Fe_{2-x}Ga_xO_3$.

We studied the angular and temperature dependences of electron spin resonance spectra obtained for a single crystal of orthorhombic $Fe_{1.1}Ga_{0.9}O_3$ (the

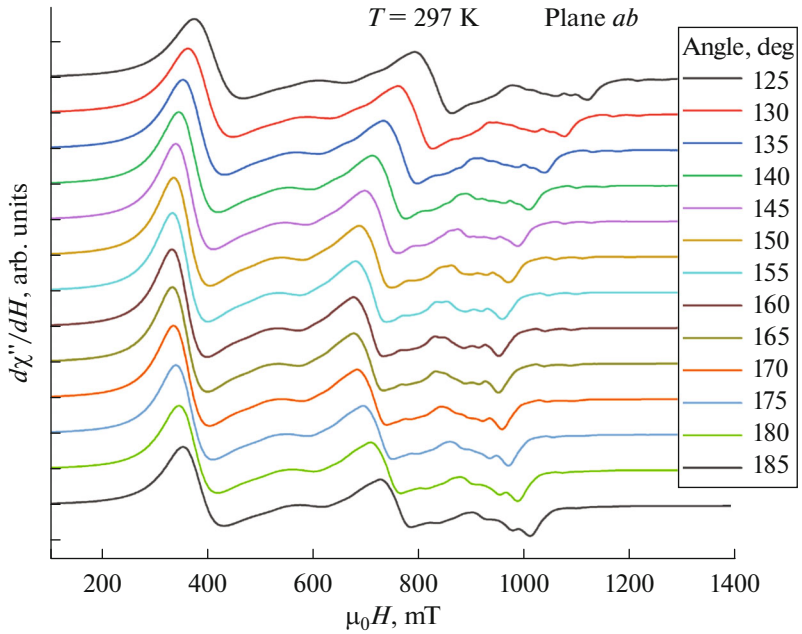

Fig. 8. Detailed consideration of the angular dependence of ESR spectra for $Fe_{1.1}Ga_{0.9}O_3$ at room temperature (297 K) in plane *ab*.

composition was determined via X-ray phase analysis) in planes *ab* and *bc*. The directions of the crystallographic axes were determined with a high level of accuracy. It was established that the considered compound was a ferrimagnet with magnetic phase transition temperature $T_C \approx 288$ K. Joint analysis of results obtained via ESR and magnetometry allowed us to estimate Curie constant $C = 2.28$ K/(cm^3 mol) and Curie–Weiss temperature $\theta_{CW} = 289$ K, even though we had no measurements of high-temperature magnetization.

Around nine lines were detected in the electron spin resonance spectra when the external magnetic field was oriented perpendicular to axis *c*, which corresponds to spin-wave resonance in an $Fe_{1.1}Ga_{0.9}O_3$ single crystal. Further studies are needed for a more detailed analysis of the ESR spectra.

ABBREVIATIONS AND NOTATION

ESR	electron spin resonance
HTCP	high-temperature crystallizing phase
ZFC	zero-field cooling mode
FC	field cooling mode
XRFA	X-ray fluorescence analysis
T	temperature
n	concentration of the crystal-forming component
H	magnetic field strength
θ_{CW}	Curie–Weiss temperature
H_{res}	position of the resonance line
T_C	temperature of the magnetic phase transition
C	Curie constant
T_{start}	initial temperature
T_{sat}	temperature of saturation
H_{res}	position of the resonance line
ΔH	line width
α	parameter of line asymmetry

ACKNOWLEDGMENTS

The authors express their gratitude to the Institute of Geology and Oil & Gas Technologies of Kazan (Privolzhskii) Federal University for allowing our investigations with X-ray fluorescence analysis.

FUNDING

This work was supported by the Russian Science Foundation, grant no. 22-12-20019 (https://rscf.ru/project/22-12-20019/), and the Krasnoyarsk Regional Science Foundation. The work of I.V. Yatsyk and R.M. Eremina was performed with the financial support from the government assignment for Federal Research Center "Kazan Scientific Center," Russian Academy of Sciences.

CONFLICT OF INTEREST

The authors of this work declare that they have no conflict of interest.

REFERENCES

1. Eremina, R.M., Moshkina, E.M., Gavrilova, T.P., et al., *Bull. Russ. Acad. Sci.: Phys.*, 2019, vol. 83, no. 7, p. 912.
2. Kurilova, A.V., Sokolov, A.E., Sukhachev, A.L., et al., *Bull. Russ. Acad. Sci.: Phys.*, 2022, vol. 86, no. 5, p. 610.
3. Tarasenko, T.N., Mikhaylov, V.I., Kravchenko, Z.F., et al., *Bull. Russ. Acad. Sci.: Phys.*, 2020, vol. 84, no. 9, p. 1113.
4. Abdrakhmanov, V.L., Zav'yalov, D.V., Konchenkov, V.I., et al., *Bull. Russ. Acad. Sci.: Phys.*, 2020, vol. 84, no. 1, p. 53.
5. Salikhov, S.V., Toleukhanova, S.K., Bordyuzhin, I.G., and Savchenko, A.G., *Bull. Russ. Acad. Sci.: Phys.*, 2019, vol. 83, no. 10, p. 1275.
6. Kalashnikova, A.M., Pisarev, R.V., Bezmaternykh, L.N., et al., *JETP Lett.*, 2005, vol. 81, no. 9, p. 452.
7. Troyanchuk, I.O., Bushinsky, M.V., Karpinsky, D.V., et al., *J. Magn. Magn. Mater.*, 2015, vol. 394, p. 212.
8. Bezmaternykh, L.N., Mashchenko, V.G., and Temerov, V.L., *J. Cryst. Growth*, 1988, vol. 87, p. 578.
9. Roy Amritendu, Mukherjee Somdutta, Gupta Rajeev, et al., *Ferroelectrics*, 2014, vol. 473, p. 154.
10. Lefevre, C., Roulland, F., Thomasson, A., et al., *J. Phys. Chem.*, 2013, vol. 117, p. 14832.
11. Kaneko, Y., Arima, T., He, J.P., et al., *J. Magn. Magn. Mater.*, 2004, vols. 272–276, p. 555.
12. Arima, T., Higashiyama, D., Kaneko, Y., et al., *Phys. Rev. B*, 2004, vol. 70, p. 064426.
13. Bakr Mohamed, M. and Fuess, H., *J. Magn. Magn. Mater.*, 2011, vol. 323, p. 2090.
14. Saha, R., Shireen, A., Shirodkar, S.N., et al., *J. Solid State Chem.*, 2011, vol. 184, p. 2353.
15. Moshkina, E.M., Gavrilova, T.P., Gilmutdinov, I.F., et al., *J. Cryst. Growth*, 2020, vol. 545, p. 125723.
16. Petrakovskii, G.A., Bezmaternykh, L.N., Velikanov, D.A., et al., *Phys. Solid State*, 2009, vol. 51, p. 2077.
17. Moshkina, E., Molokeev, M., Belskaya, N., et al., *CrystEngComm*, 2021, vol. 23, p. 6761.
18. Moshkina, E., Seryotkin, Y., Bovina, A., et al., *J. Cryst. Growth*, 2018, vol. 503, no. 1, p. 1.
19. Mukherjee, S., Garg, A., and Gupta, R., *Appl. Phys. Lett.*, 2012, vol. 100, p. 112904.
20. Moshkina, E., Ritter, C., Eremin, E., et al., *J. Phys.: Condens. Matter*, 2017, vol. 29, p. 245801.
21. Chikazumi, S., *Physics of Ferromagnetism*, New York: Oxford Univ. Press, 1997, chapters 15–17.
22. Moshkina, E., Eremin, E., Veligzhanin, A., et al., *J. Magn. Magn. Mater.*, 2023, vol. 584, p. 171072.
23. Moshkina, E.M., Molokeev, M.S., Eremin, E.V., et al., *Fiz. Tverd. Tela*, 2023, vol. 65, no. 6, p. 1054.
24. Moshkina, E.M., Belskaya, N.A., Molokeev, M.S., et al., *J. Exp. Theor. Phys.*, 2023, vol. 136, no. 1, p. 17.
25. Janhavi, P., Joshiand, S., and Bhat, V., *J. Magn. Reson.*, 2004, vol. 168, p. 284.
26. Gurevich, A.G., *Magnitnyi rezonans v ferritakh i antiferromagnetikakh* (Magnetic Resonance in Ferrites and Antiferromagnets), Moscow: Nauka, 1973.
27. Iskhakov, R.S., Stolyar, S.V., Chekanova, L.A., *Bull. Russ. Acad. Sci.: Phys.*, 2011, vol. 75, no. 2, p. 181.

Translated by O. Polyakov